Biomechanical Comparison of Vertebral Augmentation and Cement Discoplasty for the Treatment of Symptomatic Schmorl's Node Combined With Modic Change: Finite Element Analyses

Kaiwen Cai
Affiliated Hospital of Medical School Ningbo University and Ningbo City Third Hospital
Kefeng Luo
Affiliated Hospital of Medical School Ningbo University and Ningbo City Third Hospital
Feng Cao
No.906 hospital of Chinese People`s Liberation Army Joint Logistic Support Force
Bin Lu
Affiliated Hospital of Medical School Ningbo University and Ningbo City Third Hospital
Yuanhua Wu
Affiliated Hospital of Medical School Ningbo University and Ningbo City Third Hospital
Hongxia Wang
Affiliated Hospital of Medical School Ningbo University and Ningbo City Third Hospital
Kai Zhang
Affiliated Hospital of Medical School Ningbo University and Ningbo City Third Hospital
Guoqiang Jiang (jiangguoqiang@nbu.edu.cn)
Affiliated Hospital of Medical School Ningbo University and Ningbo City Third Hospital

Research article

Keywords: biomechanics, symptomatic Schmorl's node, vertebral augmentation, cement discoplasty, finite element analyses

Posted Date: March 2nd, 2021

DOI: https://doi.org/10.21203/rs.3.rs-266943/v1

Abstract

Study design: Finite element simulation study.

Objective: To compare the biomechanical effects of percutaneous vertebral augmentation (PVA) and percutaneous cement discoplasty (PCD) in patients with symptomatic Schmorl's node combined with Modic change.

Methods: CT data from a single patient was assembled into finite element models, from which we constructed four distinct surgical models, including PVA-ideal, PVA-nonideal, PCD-ideal, and PCD-nonideal, to compare the stress and strain differences of parapodular tissues.

Results: The validity of our model was confirmed. PVA-ideal model showed a moderate reduction in the stress peak of the Schmorl's node (0.48 vs. 0.81–0.89 Mpa) in the erect position. In the PCD-ideal model, the stress peak of the Schmorl's node increased significantly when the spine was moved toward the lesion (3.99Mpa). Both PVA-ideal and PCD-ideal models showed global strain inhibition at the Schmorl's node and BMEZ, which was attenuated in the non-ideal models. The PCD-ideal model significantly reduced segmental ROM (-76.8% to -59.3%) and significantly increases endplate stress (up to 220.8%), with no such effects seen in the PVA-ideal model.

Conclusions: Both PVA-ideal and PCD-ideal models facilitated a more stable parapodular biomechanical microenvironment. The PVA-ideal model yielded minimal stress disturbance on the augmented or adjacent vertebral endplate but offered no improvement to segment stability. The PCD-ideal model provides adequate segment stability, but also carries a greater risk for adjacent vertebral fracture. As nonideal implementations of both surgeries can result in poor biomechanical outcomes, the surgical indications of PVA or PCD need to be carefully selected.

Introduction

Chronic discogenic lower back pain (DLBP) is a common affliction of the middle-aged and elderly, arising as a result of age-related degeneration of the human spine. Degeneration of fibrocartilage plays an important role in the development of DLBP. Atresia of the subchondral microvascular may arise due to either this chronic degeneration or traumatic injury, which in turn leads to a loss of nutrition of the vertebral endplate [1]. Left untreated, this gradual degradation can result in endplate rupture and subchondral osteonecrosis causing the nucleus to herniate into the vertebral body under pressure, forming a Schmorl's node. Although most patients with Schmorl's nodes exhibit no obvious symptoms and are diagnosed by chance, significant correlations have been observed between abnormal MRI signals in the bone marrow (i.e., Modic type I or type II changes) around Schmorl's nodes and lower back pain [2,3]. Modic type I and type II changes indicate the existence of bone marrow edema and steatosis, respectively, but not progression into the stable type III stage. Thus, the treatment of symptomatic Schmorl's nodes combined with Modic type I or type II changes remains challenging, as this type of lesion

is usually accompanied by consistent and severe axial pain and has poor response to drugs and physical therapy [2,3].

Various therapies have been proposed for treating symptomatic Schmorl's nodes combined with Modic changes. Non-surgical treatments such as steroid injection, anti TNFα antibody therapy, antibiotics, and bisphosphonate treatment have all been shown to improve short-term outcomes, although evidence of long-term benefits remains limited [4]. Alternative therapies, such as radiofrequency ablation, are a popular treatment for DLBP, although evidence of their efficacy remains mixed [5]. Among the available treatments, lumbar fusion surgery has been shown to offer good long-term results [6]; however, the resulting loss of motion and potential risks to adjacent segments are significant concerns. Thus, alternative minimally invasive treatments have been explored.

In 2006, Masala *et al*. first reported the use of percutaneous vertebroplasty (PVP) for treating symptomatic Schmorl's nodes [7]. Soon thereafter, several researchers began experimenting with percutaneous vertebral augmentation (PVA), including PVP and percutaneous kyphoplasty (PKP), to treat this disease. PVA surgery is able to provide rapid pain relief and significant capacity improvement, which is well maintained in long-term follow-up [8–11]. In 2015, an alternative surgical approach referred to as either percutaneous cement discoplasty (PCD) or percutaneous disc cementoplasty (PDC) was first reported by Varga *et al*. [12]. This procedure was initially used to treat the disc vacuum phenomenon caused by severe degeneration of the disc, as well as vertical instability syndromes such as secondary foramen stenosis. More recently, this approach has been used to treat refractory DLBP combined with Schmorl's node or Modic changes, with satisfactory results [13–15]. These two minimally invasive methods represent significant improvements in the way we treat refractory DLBP. However, their development has been based on case series reports, with few reports of surgical-related complications. High-quality evidence regarding the safety and efficacy of these methods are therefore lacking due to the small sample sizes and high risk for conclusion bias associated with this type of research. To the best of our knowledge, no controlled studies have investigated the use of either method to date.

In this study, we compared the biomechanical effects of PVA and PCD on the human spine, assessed the effects of local stability, and identified warning signs indicative of possible surgery-related complications. This paper provides theoretical support for future research as well. Considering the uncontrollability and heterogeneity of the bone cement distribution seen in in vitro modeling, a finite element method is used to simulate the PVA/PCD procedure.

Materials And Methods

Data acquisition and reverse reconstruction

Ethical approval (KY20191103) was obtained from the ethics committee of **********, with written informed consent provided by the study volunteer.

CT data were collected from a 42-year-old male who was diagnosed with symptomatic Schmorl's node combined with Modic type I change in L_1 caudal endplate. Obvious spinal deformity, tumor, and infection were excluded. The CT parameters were 320 row dynamic volume CT (Aquilion one TSX□301A, Toshiba, JPN), tube voltage 135 KV, tube current 580 mA, slice thickness 0.5 mm, and interval 0.5 mm. Output images were saved in DCIM format. Two-dimensional images were imported into Mimics research 19.0 (Materialise, BEL) to generate 3D geometries of the affected segment (L_1) and adjacent segment (L_2), after which Geomagic Studio 2015 (Geomagic, USA) was used to perform smoothing process and solid transformation of models. The L_{1-2} disc was generated according to a CT image reference. Models of individual vertebrae were divided into cortical bone (1 mm thick) and cancellous bone. The disc model was divided into endplates (0.5 mm thick), annulus fibrosus and nucleus. In the cavity of the Schmorl's node, we observed a defect of the bone tissue, which had been filled with herniated nucleus tissue. The area of cancellous bone surrounding the Schmorl's node was defined as the bone marrow edema zone (BMEZ), which exhibited the same range of bone edema (~ 10 mm thick) as that seen in the MRI STIR image (Fig. 1). The mesh procedure was performed using Hypermesh 14.0 software (Altair Company, USA), in which the ligament and annulus fiber layers were meshed using 1D spring elements, the annulus ground and nucleus were meshed using an IsoMesh Hex8 element, and other structures were meshed by TetMesh Tet4 element.

Surgical simulation and model grouping

We set the reverse reconstruction model as the control model, as this region contained a lesion and had not yet received any treatment. For surgical models, we generated polymethyl methacrylate (PMMA) bone cement models in the vertebral body and disc to simulate PVA and PCD respectively. The composite structure of cancellous bone and PMMA was used as the reference compound due to its unique material properties.

Ideally, in PVA, the bone cement should be bowl-shaped around the Schmorl`s node and completely fill the BMEZ [7,9]. On the other hand, the intervertebral space should be filled with bone cement and expanded appropriately in PCD [12,15]. Thus, we defined the PVA-ideal and PCD-ideal models according to the above principles: PMMA completely filled in the BMEZ surrounding the node in the PVA-ideal model, and PMMA completely replacing the nucleus with the exception of the internal node space in the PCD-ideal. However, due to the uncontrollability of bone cement semifluids, nonideal distributions are commonly seen in clinical practice. We therefore developed both PVA-nonideal and PCD-nonideal models to represent these alternative distributions. In the PVA-nonideal model, similar to the common distribution of PVA, bone cement was distributed in the center of vertebrae in a dumbbell shape, while in the PCD-nonideal model, the volume of PMMA in the disc was reduced due to the residual nucleus, and the thickness of the PMMA spacer was set at 50% of the discal height. The morphological characteristics of all models are shown in Fig. 2.

Attribute assignment and load settings

Using MSC.Patran2012 software (NASA, USA), the cortical bone, cancellous bone, posterior elements, BMEZ, PMMA, PMMA-cancellous bone complex, facet cartilage, annulus fibers layers, annulus ground, and nucleus were endowed with properties as shown in Table 1 [16–20]. The anterior longitudinal ligament, posterior longitudinal ligament, ligamentum flavum, intertransverse ligament, articular capsule, interspinal ligaments, and supraspinal ligament were all simulated using 1D spring elements, all of which were reconstructed according to the normal anatomical distribution. All ligaments were set as one-way springs that were only under tension and not under pressure, with the corresponding material properties shown in Table 2 [16].

Table 1
Material parameters of each anatomical component of the models.

Materials	Elastic modulus(MPa)	Poisson's ratio
Cortical bone	12000	0.3
Cancellous bone	100	0.2
Endplate	1000	0.4
Posterior elements	3500	0.25
BMEZ	47	0.2
PMMA-cancellous complex	972	0.2
PMMA	2280	0.3
Nucleus	Hyperelastic C1 = 0.12,C2 = 0.03	
Annulus ground	8	0.45
Annulus fibers layers	500/485/420/360 (layers: 1–2/3–4/5–6/7–8)	
Facet cartilage	10	0.4

Table 2
Material parameters of ligaments of the models.

Ligaments	Strain (%)	Stiffness (N/mm)	Strain (%)	Stiffness (N/mm)	Strain (%)	Stiffness (N/mm)
Anterior longitudinal ligament	(0,12.2)	347	(12.2,20.3)	787	(20.3,+∞)	1864
Posterior longitudinal ligament	(0,11.1)	29.5	(11.1,23)	61.7	(23,+∞)	236
Articular capsule	(0,25)	36.0	(25,30)	159	(30,+∞)	384
Intertransverse ligament	(0,18.2)	0.3	(18.2,23.3)	1.8	(23.3,+∞)	10.7
Ligamentum flavum	(0,5.9)	7.7	(5.9,49)	9.6	(49,+∞)	58.2
Supraspinal ligament	(0,20)	2.5	(20,25)	5.3	(25,+∞)	34.0
Interspinal ligaments	(0,20)	1.4	(13.9,20)	1.5	(20,+∞)	14.7

Note: ligament is to generate 1D linear element structure based on the corresponding grid nodes on the mesh model. The material parameters are assigned according to the nonlinear spring element corresponding to the literature. When the strain is less than 0, its stiffness is 0, which means that it is a nonlinear structure with tension and no compression.

With the cranial endplate of L_1 set as the loading surface, we applied a preload of 300N as a simulation of body weight above L_1 and muscle strength. To avoid shear force and intervertebral rotation, the preload`s direction was set to vertically pass through the instantaneous centers of both segments [21]. The caudal end plate of L_2 was set as a fixed support, and its movement in all directions was not allowed. Six lumbar spine movements were analyzed in all models: erect, flexion, extension, left bending, right bending, left rotation, and right rotation. For all models, preload was only applied in the erect condition, with other motion conditions receiving an additional 10 N·m moment applied on the loading surface in the same direction as the motion [22].

Validation

All finite element calculations were performed using Nastran2012 software (NASA). To verify whether the spine model reconstructed in this study conformed to the mechanical properties of the real human spine, a 10 N·m bending moment was applied to the L1 cephalic endplate of the control model. The range of motion (ROM) results of flexion-extension, left-right bending, and left-right rotation were compared to the results of previous studies [22,23].

Calculations

For all six loading conditions, the Von-Mises stress and strain nephogram of the structure around the affected intervertebral space were analyzed, including the endplate, bone, bone cement, and Schmorl's node area. We also recorded any changes in stress peak and its distribution in the endplate. The ROM of the L_{1-2} segment was recorded to evaluate the segment stability of each model under each motion condition.

Results

Validation

Under the 10 N·m moment in the direction of spinal motion, the ROM of flexion-extension was 10.01°, the ROM of left-right bending was 9.64°, and the ROM of left-right rotation was 4.95°. In comparison, the equivalent ROM movements from the Yamamoto and Xiao studies were 10.4 ± 1.45°, 10.2 ± 1.5°, and 4 ± 1.7°, and 10.29°, 9.78°, and 4.02°, respectively (Fig. 3). Results of this finite element model were similar to those seen using *in vitro* specimens in terms of biomechanical characteristics and numerical values, further supporting the accuracy and efficacy of this model. Therefore, this model can be used for simulation analyses of PVA and PCD surgery in the next step.

Stress and strain at the Schmorl's node

In the erect condition, the node stress peak of the PVA-ideal model was lower than that seen in other models (0.48 vs. 0.81–0.89 Mpa), while the node stress peaks of other models were comparable. As the nodes in our models were located at the posterior of the endplate, the node stress peak significantly increased during extension in the PCD-ideal model (3.99 Mpa). In terms of strain peak at the node, the PVA-ideal and PVA-nonideal models were similar to the control. However, the nodule strain of the PVA-ideal model was primarily concentrated at the base, which makes the strain at the top of the nodules significantly smaller than that of the control model. Due to the stress shielding effect, the PCD-ideal model can significantly reduce node strain peak to 0.003, compared to 0.089 in the PCD-nonideal model, and even higher in other models. This trend was also seen when comparing the PCD-ideal and PCD-nonideal models across other spinal movement conditions (Figs. 4–6).

Stress and strain of BMEZ

In the erect condition, the BMEZ stress peaks of all models were similar; however, for other spinal movements, the BMEZ stress peak increased significantly in the PCD-ideal model, with the strongest effect seen in extension (8.72 vs. 2.34–3.09 Mpa), with an increase of 272.6%. Interestingly, both the PVA-ideal (0.003 Mpa) and PCD-ideal (0.003 Mpa) were shown to significantly reduce the strain peak of BMEZ. By contrast, the PCD-nonideal model significantly increased the strain peak of BMEZ, with the strongest differences seen for left/right bending (Figs. 4–6).

Stress of endplates

Stress peak increments of the L_1 caudal and L_2 cephalic endplates were 24.6–129.7% and 6.8–220.8%, respectively, for the PCD-ideal model, relative to controls. In comparison, the stress increments seen in other groups were all between 21.7% and 28.5%, respectively. Thus, the PCD-ideal model exhibits more extreme variation in stress under various motion conditions, particularly in regard to extension movement ((Figs. 4 and 7).

Segmental stability

The ROM values of the L_{1-2} segment of all models ranged from 0.63° to 5.66° under six motion conditions, among which the ROM of flexion, extension, left bending, right bending, left rotation, and right rotation were 2.06–5.66°, 1.77–4.59°, 1.14–4.85°, 1.12–5.58°, 0.63–2.56°, and 0.72–2.49°, respectively. The ROM of the PCD-ideal model significantly decreased (-76.8% to -59.3%), indicating more significant improvements in segmental stability relative to other groups (Table 3).

Table 3
Comparison of L_{1-2} segment ROM (°) and ROM increment relative to control(%)

Motion	Control (°)	PVA-ideal (°)(%)	PVA-nonideal (°)(%)	PCD-ideal (°)(%)	PCD-nonideal (°)(%)
Flexion	5.66	5.53 (-2.3)	5.26 (-7.1)	2.06 (-63.6)	5.30 (-6.4)
Extension	4.35	4.31 (-0.9)	4.59 (5.5)	1.77 (-59.3)	4.48 (3.0)
Left bending	4.81	4.76 (-1.0)	4.85 (0.8)	1.14 (-76.3)	4.47 (-7.1)
Right bending	4.83	4.79 (-0.8)	5.58 (15.5)	1.12 (-76.8)	5.21 (7.9)
Left rotation	2.46	2.40 (-2.4)	2.56 (4.1)	0.63 (-74.4)	2.55 (3.7)
Right rotation	2.49	2.42 (-2.8)	2.25 (-9.6)	0.72 (-71.1)	2.22 (-10.8)

Discussion

Previous studies that have examined the use of PVA and PCD in DLBP with Schmorl's node or Modic change have consistently demonstrated superior results, relative to other methods. He *et al*. followed 11 patients with a symptomatic Schmorl's node treated by PVP for an average of 58 months, and reported satisfactory long-term pain relief with no evidence of surgery-related complications [8]. Zhi-Yong *et al*. reported 32 patients treated with PKP for whom VAS, ODI, and SF-36 scores exhibited significant improvements after surgery and were well maintained over a 5-year follow-up period [10]. Of these patients, only 3 cases (6.98%) of cement disc leakage and 2 cases (4.65%) of adjacent vertebral fracture (AVF) were observed. In addition, Tian *et al*. reported that PCD treatment for patients with DBLP with Modic changes provided satisfactory outcomes, with no obvious surgical-related complications [13,14]. Based on these observations, the promise of these two minimally invasive surgical treatments have been proven. However, the evidence each of these therapies is based on a small number of case series reports,

with no randomized controlled trials used to validate these outcomes. Due to the lack of high-level evidence, theoretical demonstration of these two kinds of therapies is still necessary.

The mechanism underlying DLBP pathology includes a combination of disc pressure [24], instability [25], nerve fiber ingrowth [25,26], and release of cytokines [25,27,28]. The mechanism of pain relief achieved by PVA is thought to be mediated by a combination of strengthening and stabilization of the edema area of subchondral bone marrow, along with suspension of the processes underlying trabecular injury, and potential thermal effects [29]. On the other hand, PCD is usually used in combination with percutaneous lumbar discectomy (PLD) [13,14] in which as much of the nucleus as possible needs to be removed, which allows PCD to achieve satisfactory intervertebral stabilization and expansion. Furthermore, with the removal of the nucleus, the release of the intradiscal cytokines such as IL-1, IL-6, IL-8, PGE-2, NO, and phospholipid A2 was also resolved.

Regardless of the method used, achieving any of the pain relief described above requires an ideal distribution of bone cement. Both the PVA-ideal and PCD-ideal models facilitate a more stable parapodular biomechanical microenvironment; however, achieving this degree of bone cement diffusion is almost impossible achieve on in practice. Of the many factors that can affect bone cement distribution, the only controllable factors are injection speed and injection direction. Therefore, we also developed both PVA-nonideal and PCD-nonideal models as a means of simulating the suboptimal distribution that is more likely to occur during a PVA or PCD procedure.

In this study, a control model was used to simulate the biomechanical characteristics of the human spine under pathological conditions. Under load, the increased intradiscal pressure forces the nucleus to move toward any defect in the endplate or cortical bone. The centrifugal stress and strain in the edematous bone marrow around the Schmorl`s node in the control model is used to describe the instability of the local microstructure and the diffusion of pain causing factors. In the PVA-ideal model, this centrifugal stress and strain is blocked by the strengthened PMMA-cancellous bone complex which has a much higher elastic modulus than the edematous bone marrow. On other hand, in the PCD-ideal model, we also observed that centrifugal stress and strain were significantly diminished due to the stress-shielding effects of the PMMA in the intervertebral space, suggesting that the an elimination of the intradiscal pressure could be attributed to a combination of stress-shielding and the removal of the nucleus. The elimination of centrifugal stress and strain in the perinodal structure means that the stimulation of intradiscal cytokines to bone marrow is reduced, and the trabecular microinjury of cancellous bone is resolved. However, in the PVA-nonideal and PCD-nonideal models, the above effects are weakened. Obviously, it is impractical to expect an ideal distribution of bone cement in every surgical practice. Therefore, orthopedists need to weigh the potential risks of reduced efficacy caused by unsatisfactory distribution before the PVA/PCD surgery.

For segmental stability, the PCD-ideal model showed superior intervertebral stability, with significantly reduced ROM in all five motion directions relative to other models. By contrast, the PCD-nonideal model exhibited significantly lower stability improvement due to the incomplete filling of the intervertebral

space. Neither the PVA-ideal or PVA-nonideal models showed significant improvements in intervertebral stability relative to the control. Therefore, we consider PCD to be an effective treatment for DLBP patients with severe disc degeneration or vertical instability, consistent with previous studies [12–15].

For the stress distribution of the endplates, PVA surgery did not significantly affect either the affected endplate or the adjacent vertebral endplate. In both the PVA-ideal and PVA-nonideal models, we found only a mild effects of bone cement on endplate stress, consistent with a previous study [30]. However, the biomechanical mechanism of PCD has not been reported. In our simulation, when the high elastic modulus PMMA material completely fills the intervertebral space, the annulus fibrosus is no longer the main structure to transmit stress, which means the vast majority of stress is directly transferred to the adjacent vertebral endplate through the PMMA, resulting in significant stress-shielding. By contrast, we observed a sharp increase in endplate stress in the PCD-ideal model. As is widely known, significant intradiscal cement leakage can lead to the disc degeneration [31] and increase the risk for AVF [32,33] and should therefore be avoided. When PCD was first reported, it immediately attracted attention, and triggered extensive discussion regarding the merits of this technique. One of the core concerns is the boundary of PCD for patients with osteoporosis or spinal deformity [34,35]. The exact boundary of contraindications for PCD remains unclear. Generally, T-scores ≤ -2.5 DS in the hip, or a history of fragility fracture of the hip, wrist, or vertebrae, were considered contraindications for PCD. Moreover, despite PCD-mediated improvements in scoliotic curves, it is not recommended for severe spinal deformity [35]. Our results support the above views, with the stress of the adjacent vertebral endplate having increased 40.5% after PCD. When an additional 10 N·m bending moment is applied, the stress increase in the motion direction will reach 220.8%. This sharp increase is expected to significantly enhance the “direct pillar effect” [36] of bone cement, leading to the induction or exacerbation of AVF symptoms. Although the stress seen in the PCD-nonideal model is not as large as that seen in the PCD-ideal model, the uneven stiffness of the intervertebral disc forces the adjacent endplates to undergo uneven strain (Fig. 5), which also increases the risk for endplate collapse. Therefore, we suggest that the potential risk for PCD should be carefully considered prior to use in patients with osteoporosis.

Limitations

Our research had the following limitations. Due to the limitations of computer modeling, the cancellous bone, edema zone, PMMA, and compound were all considered homogeneous linear materials, thus the process of Schmorl’s node content entering cancellous bone under pressure could not be fully recreated in the macro model. The changes in stress and strain around Schmorl’s nodes represent the trends in cytokines release in various models. In addition, the scope of modeling was limited, with ROM results described in terms of changes in segment stability, which means this model could not be used to predict the effects on global spinal stability. We speculate that limited treatment would have only minor effects on the stability of other uninvolved segments. Finally, it was a purely theoretical study, which will require validation in clinical studies.

Conclusions

The contents of a Schmorl's node tend to herniate into the vertebral body under pressure, which can be restrained by PVA and PCD surgery. PVA conferred minimal stress disturbance on the augmented or adjacent vertebral endplates with no obvious effects on the stability of the local segments. The PCD-ideal model was shown to provide sufficient intervertebral stability, resulting in improved stress shielding of the affected disc, while stress on the adjacent vertebral endplates increased sharply. The nonideal distribution of both surgeries provided poor biomechanical improvement, which may negatively impact both the efficacy and probability of complications associated with this procedure. Surgeons must therefore consider the potential risk of bone cement not reaching the desired distribution before using these procedures. While these methods hold significant promise, the data presented here highlight the need for careful consideration of all surgical indications and risks of PVA or PCD prior to treatment.

Declarations

Acknowlegement

The authors want to thank senior engineer Bing Li for his technical support.

Funding

This work was supported by the Medical health science and technology project of Zhejiang Provincial Health Commission(2020KY872).

Conflicts of interest

All authors had no conflicts of interest to disclose.

References

1. Nachemson A, Lewin T, Maroudas A, et al. In vitro diffusion of dye through the end-plates and the annulus fibrosus of human lumbar inter-vertebral discs. Acta Orthop Scand. 1970;41 (6):589–607.
2. Takatalo J, Karppinen J, Niinimäki J, et al. Association of Modic changes, Schmorl's nodes, spondylolytic defects, high-intensity zone lesions, disc herniations, and radial tears with low back symptom severity among young Finnish adults. Spine (Phila Pa 1976). 2012 Jun 15;37 (14):1231–9.
3. Luoma K, Vehmas T, Kerttula L. Chronic low back pain in relation to Modic changes, bony endplate lesions, and disc degeneration in a prospective MRI study. Eur Spine J. 2016 Sep;25 (9):2873–81.
4. Dudli S, Fields AJ, Samartzis D, et al. Pathobiology of Modic changes. Eur Spine J. 2016 Nov;25 (11):3723–3734.
5. Leggett LE, Soril LJ, Lorenzetti DL, et al. Radiofrequency ablation for chronic low back pain: A systematic review of randomized controlled trials. Pain Res Manag. 2014 Sep-Oct;19 (5):e146–53.
6. Peng B, Chen J, Kuang Z, et al. Diagnosis and surgical treatment of back pain originating from endplate. Eur Spine J. 2009 Jul;18 (7):1035–40.

7. Masala S, Pipitone V, Tomassini M, et al. Percutaneous vertebroplasty in painful Schmorl nodes. Cardiovasc Intervent Radiol. 2006 Jan-Feb;29 (1):97–101.
8. He SC, Zhong BY, Zhu HD, et al. Percutaneous vertebroplasty for symptomatic Schmorl's nodes: 11 cases with long-term follow-up and a literature review. Pain Physician. 2017 Feb;20 (2):69–76.
9. Amoretti N, Guinebert S, Kastler A, et al. Symptomatic Schmorl's nodes: Role of percutaneous vertebroplasty – open study on 52 patients. Neuroradiol. 2019 Apr;61 (4):405–410.
10. Zhi-Yong S, Huan Z, Feng L, et al. A retrospective study of percutaneous balloon kyphoplasty for the treatment of symptomatic Schmorl's nodes: 5-year results. Med Sci Monit. 2017 Jun 13;23:2879–2889.
11. Masala S, Anselmetti GC, Marcia S, et al. Treatment of painful Modic type I changes by vertebral augmentation with bioactive resorbable bone cement. Neuroradiol. 2014 Aug;56 (8):637–45.
12. Varga PP, Jakab G, Bors IB, et al. Experiences with PMMA cement as a stand-alone intervertebral spacer: Percutaneous cement discoplasty in the case of vacuum phenomenon within lumbar intervertebral discs. Orthopade. 2015 Nov;44 Suppl 1:S1–7.
13. Tian QH, Liu ZJ, Liu HF, et al. Safety and efficacy of percutaneous lumbar discectomy and percutaneous disc cementoplasty for painful lumbar disc herniation in patients over 60 years. J Vasc Interv Radiol. 2019 Jun;30 (6):894–899.
14. Tian QH, Lu YY, Sun XQ, et al. Feasibility of percutaneous lumbar discectomy combined with percutaneous cementoplasty for symptomatic lumbar disc herniation with Modic type I endplate changes. Pain Physician. 2017 May;20 (4):E481-E488.
15. Kiss L, Varga PP, Szoverfi Z, et al. Indirect foraminal decompression and improvement in the lumbar alignment after percutaneous cement discoplasty. Eur Spine J. 2019 Jun;28 (6):1441–1447.
16. Qinjie Ling, Erxing He, Huanliang Zhang, et al. A novel narrow surface cage for full endoscopic oblique lateral lumbar interbody fusion: A finite element study. J Orthop Sci, 2019, 1–7.
17. G. Baroud, J. Nemes, P. Heini, et al. Load shift of the intervertebral disc after a vertebroplasty: A finite-element study. Eur Spine J, 2003, 12: 421–426.
18. Teng Lu, Yi Lu. Comparison of biomechanical performance among posterolateral fusion and transforaminal, extreme, and oblique lumbar interbody fusion: A finite element analysis. World Neurosurgery, 2019, 129: 890–899.
19. Cheng-Chan Lo, Kai-Jow Tsai, et al. Biomechanical differences of Coflex-F and pedicle screw fixation combined with TLIF or ALIF-a finite element study. Comput Methods Biomech Biomed Eng Imaging Vis, 2011, 14 (11): 947 -956.
20. Rohlmann A, Bauer L, Zander T, Bergmann G, Wilke HJ. Determination of trunk muscle forces for flexion and extension by using a validated finite element model of the lumbar spine and measured in vivo data. J Biomech 2006,39 (6):981–989.
21. Haddas R, Xu M, Lieberman I, et al. Finite element based-analysis for pre and post lumbar fusion of adult degenerative scoliosis patients. Spine Deform. 2019 Jul;7 (4):543–552.

22. Yamamoto I, Panjabi MM, Crisco JJ, et al. Three-dimensional movements of the whole lumbar spine and lumbosacral joint. Spine, 1989, 14 (11): 1256–1260.
23. Zhitao Xiao, Liya Wang, He Gong, et al. Biomechanical evaluation of three surgical scenarios of posterior lumbar interbody fusion by finite element analysis. Biomedical engineering online, 2012, 11 (1): 1–11.
24. Fukui D, Kawakami M, Matsumoto T, et al. Stress enhances gait disturbance induced by lumbar disc degeneration in rat. Eur Spine J. 2018 Jan;27 (1):205–213.
25. Ohtori S, Miyagi M, Inoue G. Sensory nerve ingrowth, cytokines, and instability of discogenic low back pain: A review. Spine Surg Relat Res. 2018 Jan 27;2 (1):11–17.
26. Freemont AJ, Peacock TE, Goupille P, et al. Nerve ingrowth into diseased intervertebral disc in chronic back pain. Lancet. 1997 Jul 19;350 (9072):178–81.
27. Molinos M, Almeida CR, Caldeira J, et al. Inflammation in intervertebral disc degeneration and regeneration. J R Soc Interface. 2015 Jul 6;12 (108):20150429.
28. Cohen SP, Mao J. Neuropathic pain: Mechanisms and their clinical implications. BMJ. 2014 Feb 5;348:f7656.
29. Toksvig-Larsen S, Johnsson R, Strömqvist B. Heat generation and heat protection in methylmethacrylate cementation of vertebral bodies. A cadaver study evaluating different clinical possibilities of dural protection from heat during cement curing. Eur Spine J. 1995;4 (1):15–7.
30. Rohlmann A, Zander T, Bergmann G. Spinal loads after osteoporotic vertebral fractures treated by vertebroplasty or kyphoplasty. Eur Spine J. 2006 Aug;15 (8):1255–64.
31. Jamjoom B, Patel S, Bommireddy R, Klezl Z. Impact of the quantity of intradiscal cement leak on the progression of intervertebral disc degeneration. Ann R Coll Surg Engl. 2017 Sep;99 (7):529–533.
32. Seo DH, Oh SH, Yoon KW, et al. Risk factors of new adjacent compression fracture after percutaneous vertebroplasty: Effectiveness of bisphosphonate in osteoporotic or osteopenic elderly patients. Korean J Neurotrauma. 2014 Oct;10 (2):86–91.
33. Rho YJ, Choe WJ, Chun YI. Risk factors predicting the new symptomatic vertebral compression fractures after percutaneous vertebroplasty or kyphoplasty. Eur Spine J, 2012, 21 (5): 905911.
34. Wang B, Shan L, Hao D. Letter to the Editor concerning “Percutaneous cement discoplasty for the treatment of advanced degenerative disk disease in elderly patients” by Sola C, Camino Willhuber G, Kido G et al. Eur Spine J. 2018 Jul;27 (7):1665–1666.
35. Camino Willhuber G, Sola C. Answer to the Letter to the Editor of Biao Wang et al. concerning “Percutaneous cement discoplasty for the treatment of advanced degenerative disk disease in elderly patients” by Sola C, Camino Willhuber G, Kido G et al. Eur Spine J. 2018 Jul;27 (7):1667–1668.
36. Ahn Y, Lee JH, Lee HY, et al. Predictive factors for subsequent vertebral fracture after percutaneous vertebroplasty. J Neurosurg Spine. 2008 Aug;9 (2):129–36.

Figures

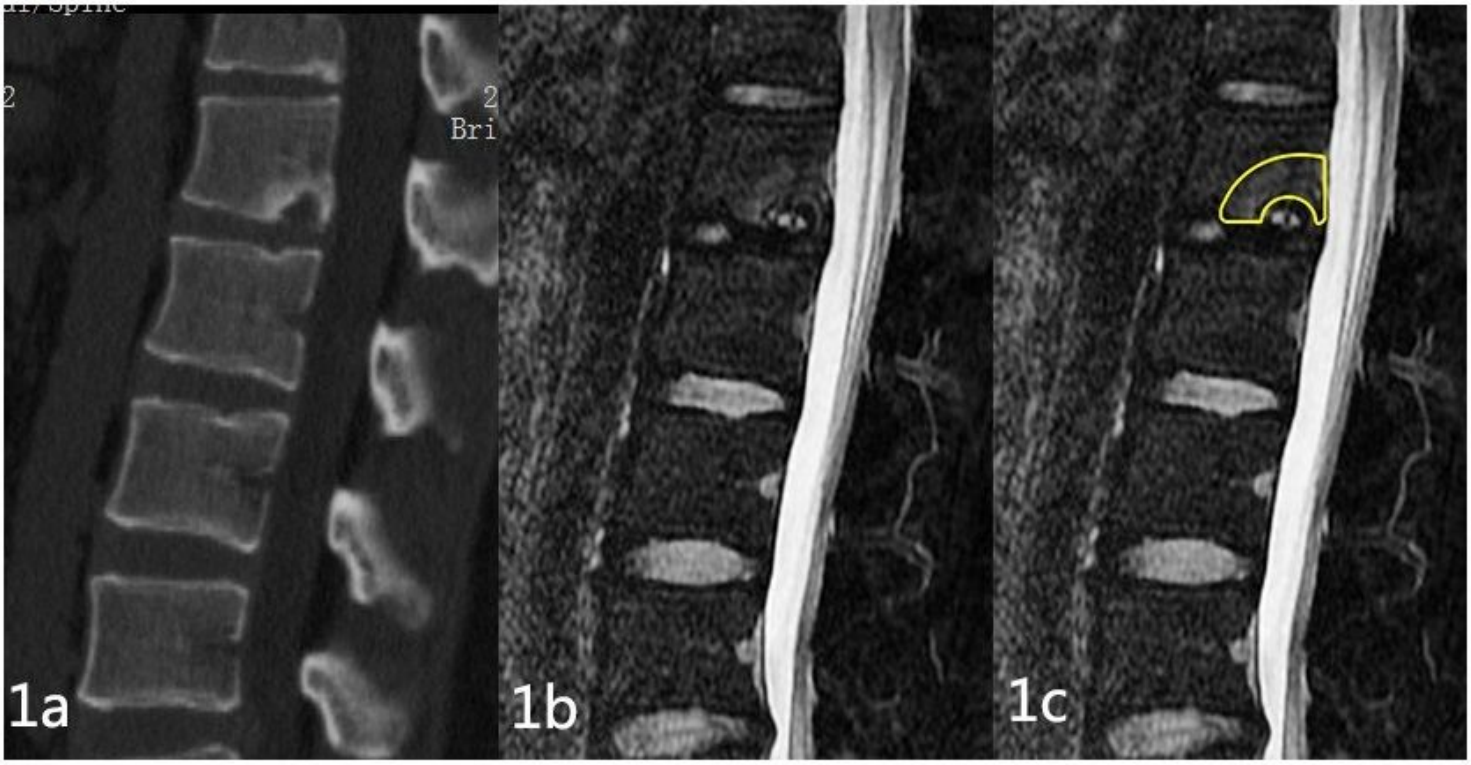

Figure 1

Imaging data of volunteer. (a) Sagittal CT of spine showed existence of Schmorl's node in L1 caudal endplate. (b) MRI STIR image showed the range of Modic type changes. (c) The range of the yellow circle mark is set as BMEZ.

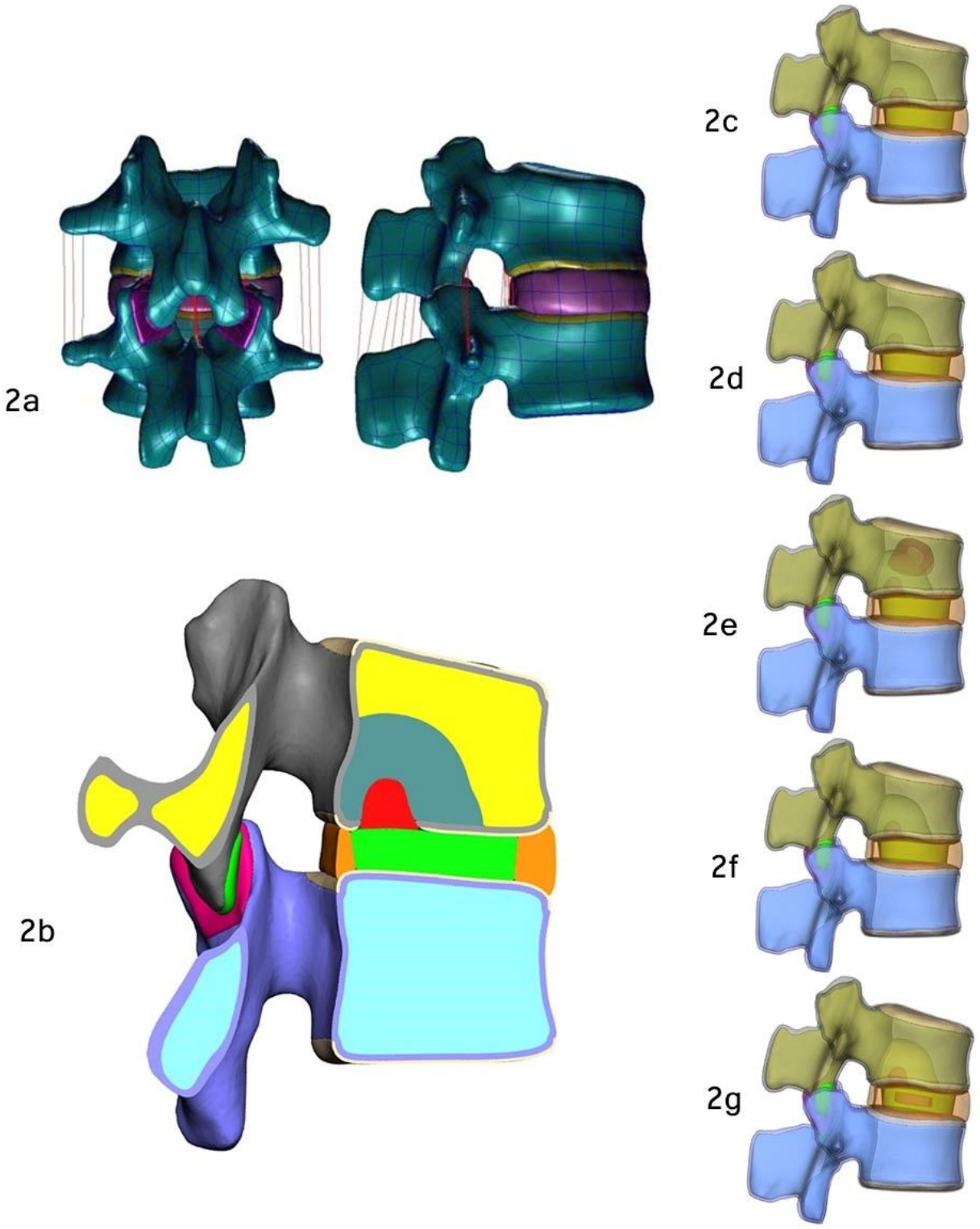

Figure 2

Reconstruction model of volunteer spine. (a) Back view and side view. (b) Section view. (c) Control model(without any therapy). (d) PVA-ideal model, PMMA completely filled in the BMEZ. (e) PVA-nonideal model, PMMA distributed in the center of vertebral as a dumbbell shape. (f) PCD-ideal model, PMMA completely replaced the nucleus. (g) PCD-nonideal model, PMMA partly replaced the nucleus.

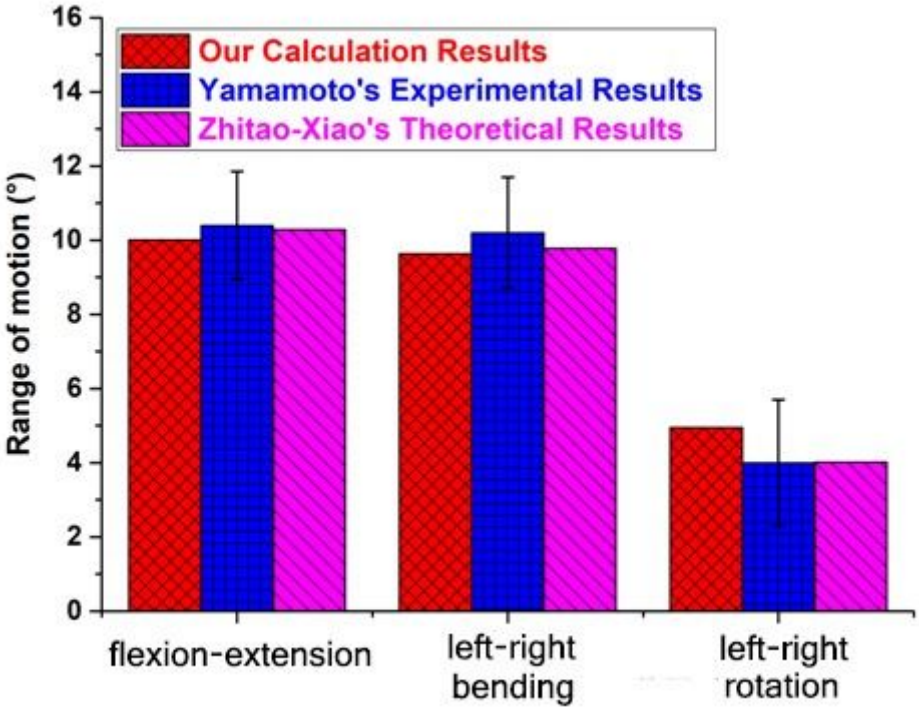

Figure 3

The mechanical verification of the control model in this study shows that it has good biomechanical simulation.

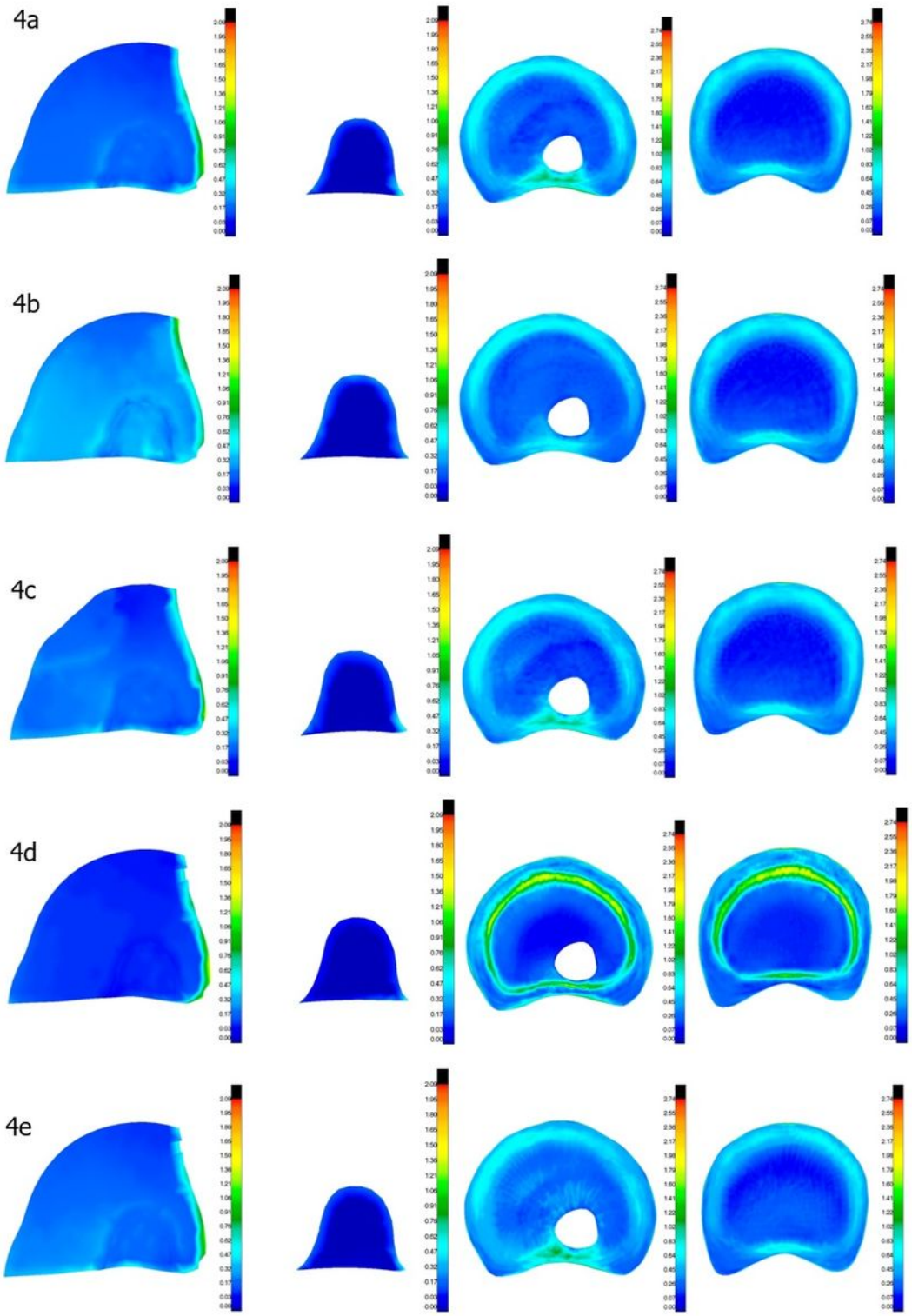

Figure 4

Stress nephogram of perinodular tissue. (a) Stress nephogram of BMEZ, Schmorl's node, L1 caudal endplate and L2 cephalic endplate in control model. (b) Stress nephogram of BMEZ, Schmorl's node, L1 caudal endplate and L2 cephalic endplate in PVA-ideal model. (c) Stress nephogram of BMEZ, Schmorl's node, L1 caudal endplate and L2 cephalic endplate in PVA-nonideal model. (d) Stress nephogram of BMEZ, Schmorl's node, L1 caudal endplate and L2 cephalic endplate in PCD-ideal model. (e) Stress

nephogram of BMEZ, Schmorl's node, L1 caudal endplate and L2 cephalic endplate in PCD-nonideal model.

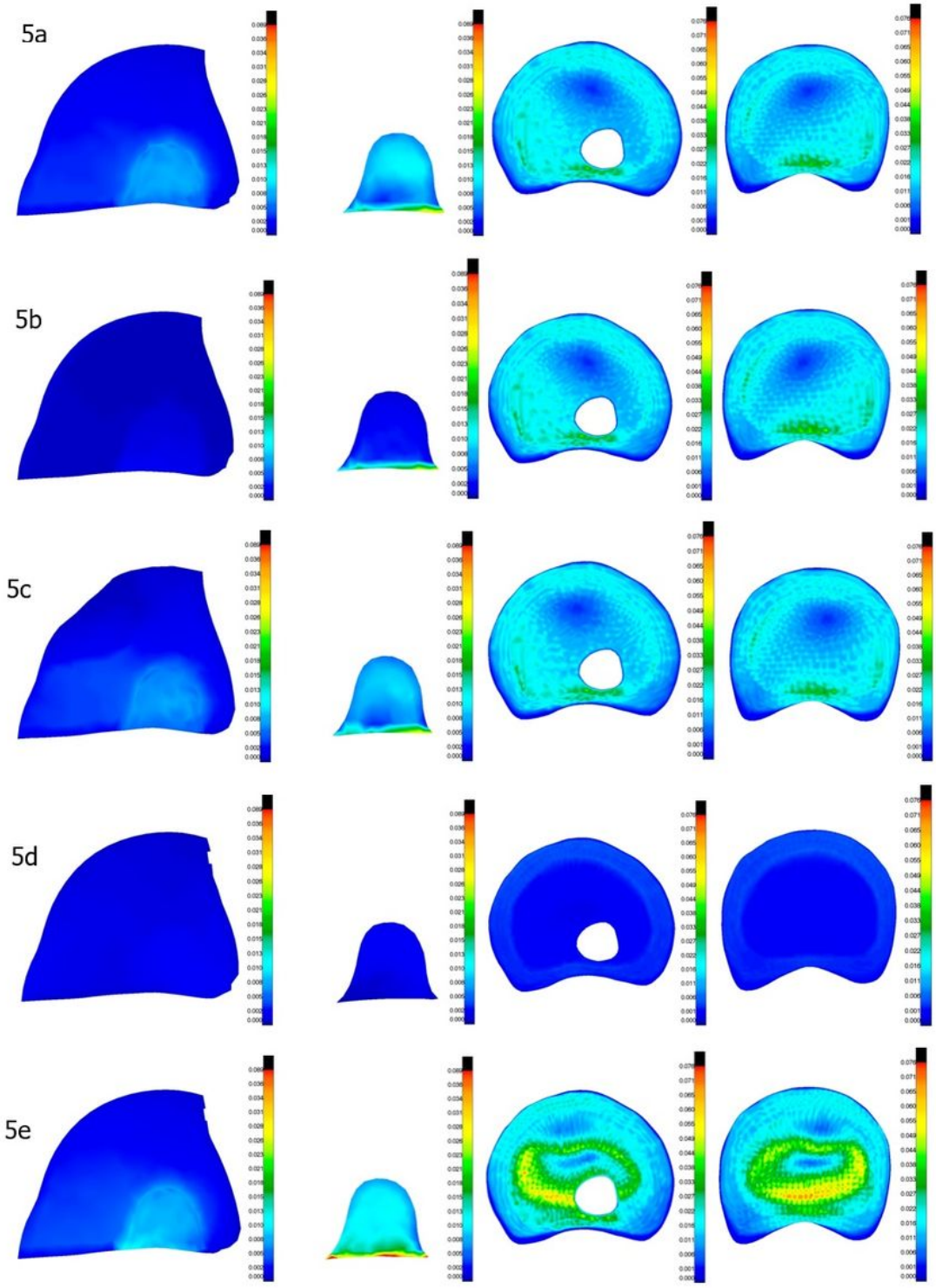

Figure 5

Strain nephogram of perinodular tissue. (a) Strain nephogram of BMEZ, Schmorl's node, L1 caudal endplate and L2 cephalic endplate in control model. (b) Strain nephogram of BMEZ, Schmorl's node, L1 caudal endplate and L2 cephalic endplate in PVA-ideal model. (c) Strain nephogram of BMEZ, Schmorl's

node, L1 caudal endplate and L2 cephalic endplate in PVA-nonideal model. (d) Strain nephogram of BMEZ, Schmorl's node, L1 caudal endplate and L2 cephalic endplate in PCD-ideal model. (e) Strain nephogram of BMEZ, Schmorl's node, L1 caudal endplate and L2 cephalic endplate in PCD-nonideal model.

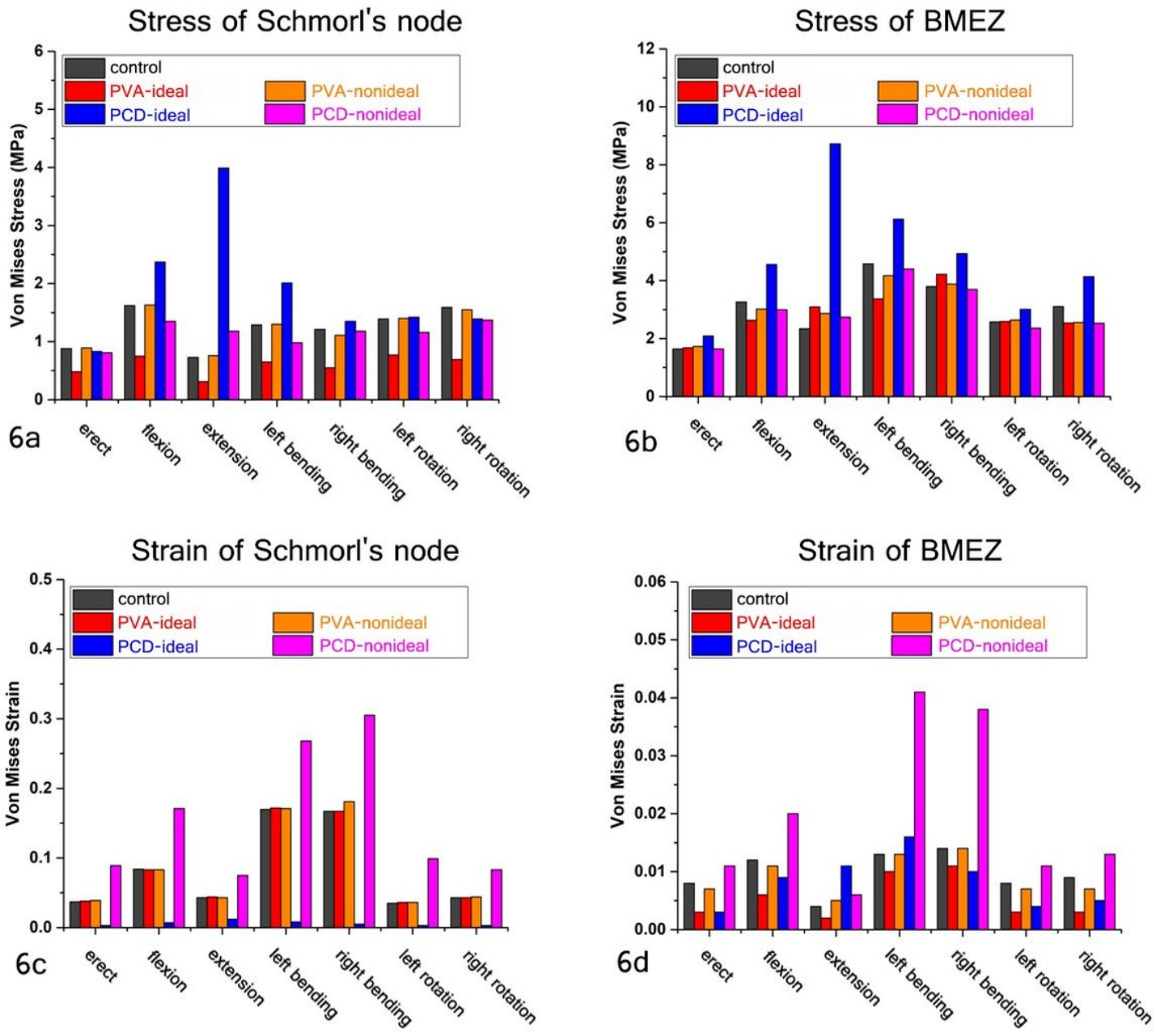

Figure 6

Stress and strain of Schmorl`s node and BMEZ.

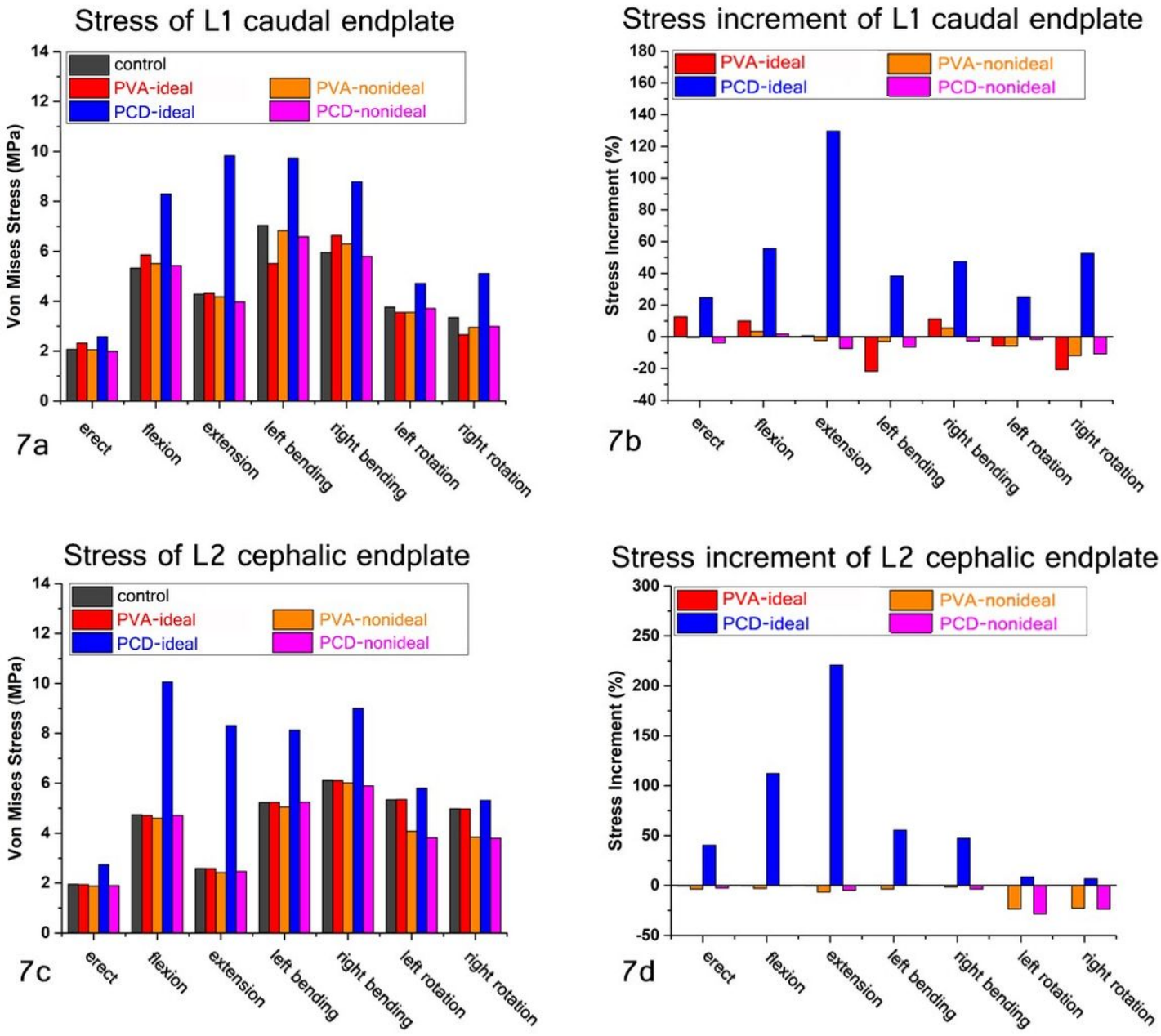

Figure 7

Stress of affected endplate.